

# TimeSenCLIP: A Vision-Language Model for Remote Sensing Using Single-Pixel Time Series

Pallavi Jain<sup>1, 2, 6</sup>, Diego Marcos<sup>2, 6</sup>, Dino Ienco<sup>2, 3, 5, 6</sup>, Roberto Interdonato<sup>2, 4, 5, 6</sup>, and Tristan Berchoux<sup>1, 5, 6</sup>

<sup>1</sup>Mediterranean Agronomic Institute of Montpellier - CIHEAM-IAMM, <sup>2</sup>Inria, <sup>3</sup>INRAE,

<sup>4</sup>Cirad, <sup>5</sup>UMR TETIS, <sup>6</sup>Univ. of Montpellier, Montpellier, France

{pallavi.jain, diego.marcos, dino.ienco, roberto.interdonato}@inria.fr

berchoux@iamm.fr

**Keywords:** VLMs, Time-Series, Multispectral, Remote Sensing, Sentinel-2, Cross-View, Contrastive learning

## Abstract

Vision-language models have shown significant promise in remote sensing applications, particularly for land-use and land-cover (LULC) via zero-shot classification and retrieval. However, current approaches face two key challenges: reliance on large spatial tiles that increase computational cost, and dependence on text-based supervision, which is often not readily available. In this work, we present TimeSenCLIP, a lightweight framework that reevaluate the role of spatial context by evaluating the effectiveness of a single pixel by leveraging its temporal and spectral dimensions, for classifying LULC and ecosystem types. By leveraging spectral and temporal information from Sentinel-2 imagery and cross-view learning with geo-tagged ground-level photos, we minimises the need for caption-based training while preserving semantic alignment between overhead (satellite) and ground perspectives. Our approach is grounded in the LUCAS and Sen4Map datasets, and evaluated on classification tasks including LULC, crop type, and ecosystem type. We demonstrate that single pixel inputs, when combined with temporal and spectral cues, are sufficient for thematic mapping, offering a scalable and efficient alternative for large-scale remote sensing applications. Code is available at <https://github.com/pallavijain-pj/TimeSenCLIP>

## 1. Introduction

Remote sensing technology is central to large-scale environmental monitoring, providing critical insights into land cover change, ecosystem health, biodiversity assessment, and agricultural productivity (Li et al., 2014, Soubry et al., 2021). The use of machine learning for the enhanced analysis of satellite data has enabled increasingly automated and accurate classification systems. However, the challenge of scaling out across diverse ecosystems, sensing modalities, and geographical regions remains largely unresolved, particularly when computational efficiency and generalization to unseen classes are required (Reichstein et al., 2019, Zhu et al., 2017, Qiu et al., 2024, Tan et al., 2024).

Recent advances in vision-language models (VLMs) have opened new possibilities in this domain. Models like CLIP (Radford et al., 2021), which learn aligned embeddings between images and natural language, have shown remarkable zero-shot generalization across a wide range of vision tasks such as object recognition, semantic segmentation, image captioning, and cross-modal retrieval (Tschannen et al., 2025). When adapted to remote sensing, VLMs allows for open-vocabulary classification and text-driven retrieval of overhead imagery data using natural language queries (e.g., “arid farmland with sparse vegetation” or “oil palm plantations near waterways”), significantly reducing the need for exhaustive, class-specific supervision (Dhakal et al., 2023, Jain et al., 2025, Mall et al., 2023, Vivanco Cepeda et al., 2023, Klemmer et al., 2025).

This capability is particularly appealing for ecosystem mapping, which extends beyond traditional land-use and land-cover (LULC) classification (e.g., “urban” or “cropland”), by combining diverse biophysical information to produce thematic maps that depict the spatial distribution, scale, and eco-

logical linkages of natural systems within a given landscape (e.g., for mapping biodiversity, habitat, and ecological regions) (Keith et al., 2022, Lausch et al., 2016). Such distinctions are often fine-grained, context-dependent, and not well captured by fixed-class LULC taxonomies. Addressing this complexity typically requires either labor-intensive expert annotation or flexible models capable of adapting to unseen descriptions. VLMs bridge this gap by interpreting open-ended text prompts to identify nuanced classes without retraining (eg. “old-growth mangrove forest near coastal region” versus simply “mangrove”) (Sastry et al., 2025, Jain et al., 2025).

Despite this promise, deploying VLMs in remote sensing presents two major challenges. **Firstly**, reliance on caption-based supervision. Many VLMs require aligned image-text pairs for training or fine-tuning. While text-labeled datasets are increasingly available in remote sensing (Zhang et al., 2023, Qu et al., 2016, Lu et al., 2017), they suffer from several limitations: they are labor-intensive to create, prone to human bias, and constrained by a fixed vocabulary. This makes them ill-suited for open-world ecological modeling, where rare classes, local naming conventions, or visually similar ecosystems, challenge closed-vocabulary systems. Consequently, such models may fail to generalize to underrepresented ecological phenomena or novel class distributions.

**Secondly**, dependence on large spatial contexts. Many remote sensing models inherit from their general computer vision counterparts a reliance on relatively large spatial contexts, often using input patches of several hundred pixels (e.g.,  $200 \times 200$  to  $512 \times 512$  pixel patches) (Zhang et al., 2016, Zhu et al., 2017). This is assumed to be useful because spatial neighborhoods provide valuable cues about LULC, or ecosystem types. While this assumption holds true in cases where spatial patterns are distinctive, especially in very high-resolution imagery, it also leads to increased computational and storage costs. Moreover,

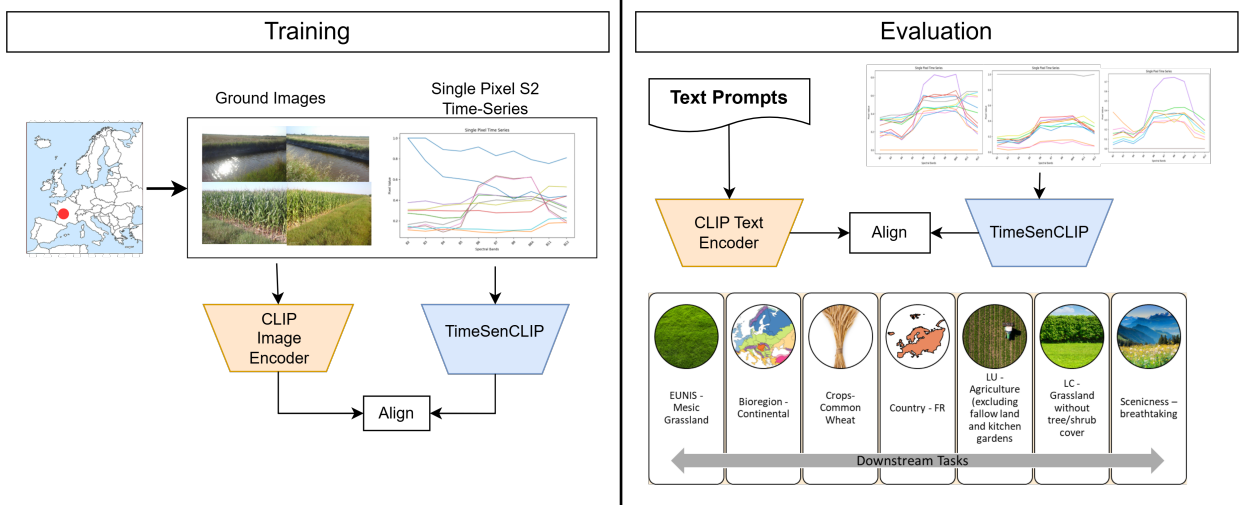


Figure 1. The infographic illustrates the training and evaluation pipeline of the TimeSenCLIP model. During training, ground-level images and Sentinel-2 single pixel time-series data from the same geographical location are aligned to learn a shared representation using a CLIP image encoder and the TimeSenCLIP module. In the evaluation phase, the trained TimeSenCLIP (for time-series) and CLIP text encoder (for text prompts) are employed to support a wide range of downstream tasks such as land cover classification, crop type identification, bioregion mapping, habitat mapping and scenicness assessment.

when spatial resolution is coarser (e.g., Sentinel-2 or Landsat), or under challenging conditions such as cloud cover, seasonal occlusion, or tasks with weak spatial autocorrelation (Koldasbayeva et al., 2024), a large spatial context may introduce noise rather than improve classification performance. These challenges are further compounded in multimodal settings involving multispectral and temporal data, which add to the volume, dimensionality, and processing complexity.

To address these challenges, we propose a VLM-based framework designed to operate with minimal spatial context and no textual supervision. Specifically, we investigate whether single-pixel time series from Sentinel-2 imagery contain sufficient information to support accurate classification across several tasks related to LULC and ecosystem type mapping. This question probes the longstanding assumption that broader spatial context is necessary and instead emphasizes spectral and temporal richness as a core signal in remote sensing. To further investigate the role of spatial context, we conduct an ablation study by increasing the patch size to  $5 \times 5$  and  $9 \times 9$ , analysing whether incorporating neighbouring pixels enhances performance and to what extent this added context is meaningful for LULC and ecosystem mapping tasks.

By reducing its spatial footprint, our model could dramatically lower computational and storage demands, paving the way for scalable, low-cost, and lightweight remote sensing models that are deployable in real-world settings.

Rather than relying on text labels, we adopt a cross-view learning paradigm that aligns satellite imagery with geo-tagged ground-level images. Inspired by works like SenCLIP (Jain et al., 2025), Sat2Cap (Dhakal et al., 2023), GRAFT (Mall et al., 2023), this approach leverages visual supervision across modalities: ground images provide rich visual semantics of local environments, aligned with text representations via generic VLMs such as CLIP, while satellite images capture the corresponding spectral-temporal signature from above. By aligning these two views in a shared embedding space, our model learns robust representations of satellite features without requiring text-

based annotations. This strategy enables open-set generalization and alleviates the limitations of fixed-vocabulary captioning. Moreover, it allows the model to capture hidden semantics such as vegetation structure, land use, or habitat composition, which may not be easy to describe through natural language alone.

In contrast to previous work, we incorporate the multi-spectral and temporal dimensions of remote sensing imagery, and show their usefulness in a range of ecological and agricultural applications such as crop mapping, bioregion delineation, and habitat and LULC classification. These tasks benefit significantly from spectral diversity and temporal dynamics that reveal phenological patterns and subtle spectral shifts (Zhong et al., 2019, Rußwurm and Körner, 2018, Lausch et al., 2016, Pettorelli et al., 2016, Pesaresi et al., 2022). However, the integration of rich spectral and temporal information significantly increases computational and processing demands. To address this, our approach consists of minimizing the spatial context provided to the model, striking a balance between predictive performance and computational efficiency.

For this study, we utilized the LUCAS 2018 dataset (d'Andrimont et al., 2020), which provides geo-tagged ground-level images alongside detailed LULC annotations across Europe. The LUCAS dataset is a well-established resource for field-based validation and includes metadata related to vegetation and crop types, as well as LULC characteristics at each location. To complement this ground-level perspective, we incorporated the Sen4Map (Sharma et al., 2024) dataset (derived from Sentinel-2 imagery and aligned with LUCAS geo-tags), which includes annual composite satellite images with 10 spectral bands and  $64 \times 64$  pixels.

In order to extend the evaluation beyond the LULC classes provided by LUCAS, we extended the test dataset by integrating additional environmental attributes. Specifically, each geo-tagged point was associated with its corresponding biogeographical region (European Environment Agency, 2016) and EUNIS (European Nature Information System) ecosystem clas-

sification (European Environment Agency, 2019). This enrichment adds another layer of ecological semantics, enabling a more nuanced evaluation of our models. By grounding our experiments in this robust, multi-source dataset, we aim to assess the generalizability of remote sensing VLMs across diverse geographical contexts (e.g., different biogeographical regions throughout Europe) and semantic categories (e.g., ecosystem types, land cover classes, crop types).

Our contributions are threefold: (1) the use of temporal cross-view learning with geo-tagged ground imagery as an alternative to caption-based supervision, (2) a comprehensive analysis of the minimal spatial context necessary for accurate ecosystem and LULC classification using VLMs, specifically in the context of Sentinel-2 imagery, where moderate spatial resolution (10–20 m) limits the utility of fine-grained spatial features, and (3) an evaluation of a temporally and spectrally-informed VLM variant designed to improve robustness across key remote sensing tasks, including LULC classification, EUNIS habitat mapping, and crop type identification. Together, these contributions aim to improve the scalability, efficiency, and adaptability of ecosystem and LULC mapping methods in data-constrained environments.

## 2. Related Works

Our approach builds upon recent advances in remote sensing foundation models, vision-language alignment, and multivariate time series learning, but departs from prior work through its architectural asymmetry, temporal augmentation strategies, and exclusive use of image-based contrastive supervision, without prompt-based or text-driven objectives.

### 2.1 VLMs in Remote Sensing

VLMs such as CLIP (Radford et al., 2021) have transformed zero-shot learning by projecting images and text into a shared embedding space, enabling flexible and scalable classification across diverse domains. Inspired by these advances, recent efforts have adapted VLMs to the remote sensing domain. Notable examples include GeoRSCLIP (Zhang et al., 2023), SkyCLIP (Wang et al., 2024), and RemoteCLIP (Liu et al., 2023), which leverage satellite imagery and natural language to perform open-vocabulary land cover classification. These models demonstrate strong generalization by pairing large-scale remote sensing imagery with curated textual descriptions. Beyond classification, models like GeoPixel (Shabbir et al., 2025) extend vision-language alignment to the pixel and patch level, enabling fine-grained captioning and grounding over high-resolution Earth observation data. However, such models often assume that semantic understanding can only emerge from larger spatial contexts. This is reflected in the use of large image patches (e.g.,  $224 \times 224$  pixels), which implicitly rely on local spatial continuity for semantic inference. While effective in many structured environments, this assumption becomes problematic in ecologically diverse or fragmented landscapes, such as mixed-crop, hedgerow mosaics, agroforestry systems, seasonal floodplain wetlands, or shrub-steppe regions, where spatial coherence is weak, discontinuous, or even misleading. A second limitation lies in their reliance on caption-based supervision; training typically depends on manually curated image–text datasets (e.g., RS5M (Zhang et al., 2023)), which are costly to scale and often suffer from vocabulary bias, especially in underrepresented ecological contexts.

Our work challenges these assumptions by exploring whether rich semantics can emerge from minimal spatial context such as single pixel patches, when paired with spectral-temporal signatures. We demonstrate that, without relying on large spatial extent or handcrafted text prompts, small inputs encode sufficient information to support ecosystem retrieval and alignment.

### 2.2 Cross-View Ground–Satellite Alignment

Cross-view supervision has emerged as a compelling strategy for learning geospatial representations by aligning overhead (satellite) and ground-level imagery. Models such as Sat2Cap (Dhakal et al., 2023), SenCLIP (Jain et al., 2025), and GRAFT (Mall et al., 2023) leverage contrastive or generative objectives to bridge the domain gap between views. SenCLIP, in particular, introduces an attention pooling mechanism across directional ground-level images, processed via a frozen CLIP encoder and aligns them with Sentinel-2 inputs, inspiring the ground encoder design in our model. Similarly, GAIR (Liu et al., 2025) applies hierarchical fusion of satellite and ground imagery to learn coherent geospatial embeddings for downstream tasks.

In contrast to these approaches, we propose to align spectral-temporal patches from Sentinel-2 with ground-level features through direct contrastive learning, avoiding any reliance on spatial priors, or language-based objectives. This enables learning from extremely small spatial inputs (as little as single pixel), while retaining semantic richness from high-resolution ground imagery. Our model thereby offers a supervision efficient alternative for geospatial representation learning, applicable across ecological, agricultural, and other land-use domains.

### 2.3 Multispectral and Temporal Remote Sensing Models

Recent advances in spectral-temporal VLMs for remote sensing have shown promising results. Some notable examples include Llama3-MS-CLIP, which extends RGB patches to multispectral inputs (Marimo et al., 2025); GeoLLAVA, which frames time series as video-language pairs (Elgendi et al., 2024); and EarthDial, which adopts a two-stage strategy of RGB-to-multispectral and temporal fine-tuning (Soni et al., 2024). These methods demonstrate partial progress, but remain limited by their reliance on RGB priors, fixed temporal windows, or supervised fine-tuning. In contrast, our transformer-based framework directly processes raw spectral-temporal cubes through mechanisms that jointly model multispectral (10 Sentinel-2 channels) and multi-temporal information, without requiring text prompts, spatial upsampling, or separate pretraining stages. This integrated approach captures useful phenological patterns and spectral dynamics that conventional VLMs do not capture.

### 2.4 Ecological Representation and Remote Sensing Foundations

Recent work has advanced ecological representation learning by aligning remote sensing imagery with external ecological knowledge. For example, EcoWiKiRS (Zermatten et al., 2025) and TaxaBind (Sastry et al., 2025) leverage species occurrence data and habitat types, while WildSAT (Daroya et al., 2024) predicts biodiversity indicators directly from satellite inputs. Other efforts explore multi-sensor fusion for ecosystem modelling (Wang et al., 2025).

Our approach contributes a minimalist alternative, without requiring class labels, taxonomies, or curated prompts, by aligning Sentinel-2 spectral–temporal patches with image-level supervision from ground-level imagery. It avoids spatial priors or dense annotations (e.g., segmentation maps), and instead learns directly from raw overhead pixels (as small as  $1 \times 1$ ) through cross-view supervision.

This setup enables rich semantic representations to emerge from spectral–temporal structure alone, supporting a broader shift toward scalable, data-driven ecosystem modelling in remote sensing VLMs.

### 3. Method

Our architecture, TimeSenCLIP (Temporal-Spectral VLM for Sentinel-2 imagery), as shown in Figure 2, builds upon the principles established in prior cross-view and satellite-ground alignment works, such as SenCLIP (Jain et al., 2025), Sat2Cap (Dhakal et al., 2023), and GRAFT (Mall et al., 2023). While these methods primarily rely on CLIP-based (Radford et al., 2021) encoders for both views, we train the satellite encoder from scratch to enable: (1) flexible spatial patch sizes for overhead images to handle minimal spatial context, and (2) exploiting multi-spectral and temporal dimensions.

#### 3.1 Model Overview

TimeSenCLIP consists of two image encoders i.e. ground-level encoder and satellite encoder. Ground-level images are encoded using a frozen CLIP encoder  $f_G$ , followed by a learnable pooling operation to obtain the ground embedding  $G_i$ . Sentinel-2 multispectral time series patches are encoded using a ViT-based temporal encoder  $f_S$ , which receives linear patch embeddings, temporal-position encodings, and a CLS token. The model is trained using a contrastive loss, aligning spectral-temporal embeddings  $S_i$  with corresponding ground embedding pair  $G_i$  while using a memory queue of negatives to compute similarity scores.

**Ground-level Encoder.** We retain the CLIP image encoder  $f_G(\cdot)$  as a frozen feature extractor, leveraging its strong visual priors learned from natural image corpora. For each geographic location, we utilize four geo-tagged directional images  $\{Y_G^n, Y_G^e, Y_G^s, Y_G^w\}$ . These are independently encoded by the frozen CLIP encoder and apply an attention pooling mechanism as introduced in SenCLIP, to produce a unified embedding:

$$\mathbf{g} = \text{AttnPool}([f_G(Y_G^n), f_G(Y_G^e), f_G(Y_G^s), f_G(Y_G^w)])$$

**Satellite Encoder.** For the **Sentinel-2 time series**, we design a transformer-based model  $f_S(\cdot)$  that takes as input a spectral-temporal cube  $\mathbf{X} \in \mathbb{R}^{T \times C \times H \times W}$ , where  $T$  denotes the number of temporal frames,  $C$  is the number of spectral bands, and  $H \times W$  is the spatial extent. Each time slice  $X_t \in \mathbb{R}^{C \times H \times W}$  is flattened and projected with a linear layer:

$$\mathbf{x}_t = \text{Linear}(\text{Flatten}(X_t)), \quad t = 1, \dots, T$$

To improve robustness to incomplete or irregular temporal sequences (e.g., due to missing observations or inconsistent

sampling), we apply a temporal augmentation strategy (temporal dropout).

After temporal augmentation, learnable temporal position embeddings  $\mathbf{p}_t$  are added to each remaining time step, and a learnable *class token*  $\mathbf{cls}$  is prepended to the sequence:

$$\mathbf{z} = [\mathbf{cls}; \mathbf{x}_1 + \mathbf{p}_1; \dots; \mathbf{x}_T + \mathbf{p}_T]$$

The full sequence is then processed by the Transformer encoder  $f_S(z)$ . From the output, the embedding corresponding to the class token  $\mathbf{cls}$  is extracted as the initial satellite representation. To enhance this temporal embedding, we adopt a lightweight multi-layer perceptron (MLP) head to further refine the output of the Transformer:

$$\mathbf{s} = \text{MLPHead}(f_S(\mathbf{z}))$$

**Cross-modal Alignment with Contrastive Learning.** We adopt an InfoNCE-based contrastive learning setup, where ground-level image embeddings remain frozen, while the satellite encoder is trained to align with them. Let  $s$  be the satellite image time series embedding and  $g$  the ground level image embedding. We compute the L2-normalized embeddings of dimension  $d$ :

$$\mathbf{z}_S = \frac{\mathbf{s}}{\|\mathbf{s}\|_2}, \quad \mathbf{z}_G = \frac{\mathbf{g}}{\|\mathbf{g}\|_2}$$

To scale training beyond in-batch negatives, we incorporate a MoCo-style (He et al., 2020) memory bank  $\mathcal{Q} \in \mathbb{R}^{K \times d}$  that stores ground embeddings. The contrastive logits are computed as:

$$\text{logits} = [\mathbf{z}_S \cdot \mathbf{z}_G, \mathbf{z}_S \cdot \mathbf{q}_1, \dots, \mathbf{z}_S \cdot \mathbf{q}_K] \in \mathbb{R}^{1+K}$$

where the first term represents the positive pair similarity, and the remaining  $K$  terms are dot products with negatives from the queue  $q$ . The final InfoNCE loss is then:

$$\mathcal{L}_{\text{InfoNCE}} = -\log \frac{\exp(\mathbf{z}_S \cdot \mathbf{z}_G / \tau)}{\exp(\mathbf{z}_S \cdot \mathbf{z}_G / \tau) + \sum_{i=1}^K \exp(\mathbf{z}_S \cdot \mathbf{q}_i / \tau)}$$

where  $\tau$  is a learnable temperature parameter, the denominator includes both positive and negative pairs (via a momentum-based queue).

#### 3.2 Dataset

**Cross-View Dataset** The LUCAS survey is a European Union-wide land cover and land use field campaign conducted in 2018 (d’Andrimont et al., 2020), comprising approximately 235,000 geo-tagged rural locations. Each site is documented with high-resolution ground-level images taken in four cardinal directions (north, east, south, and west), accompanied by detailed annotations of land use, land cover (LULC), and crop types.

For the remote sensing imagery, we utilized the Sen4Map dataset (Sharma et al., 2024), which provides multi-spectral and

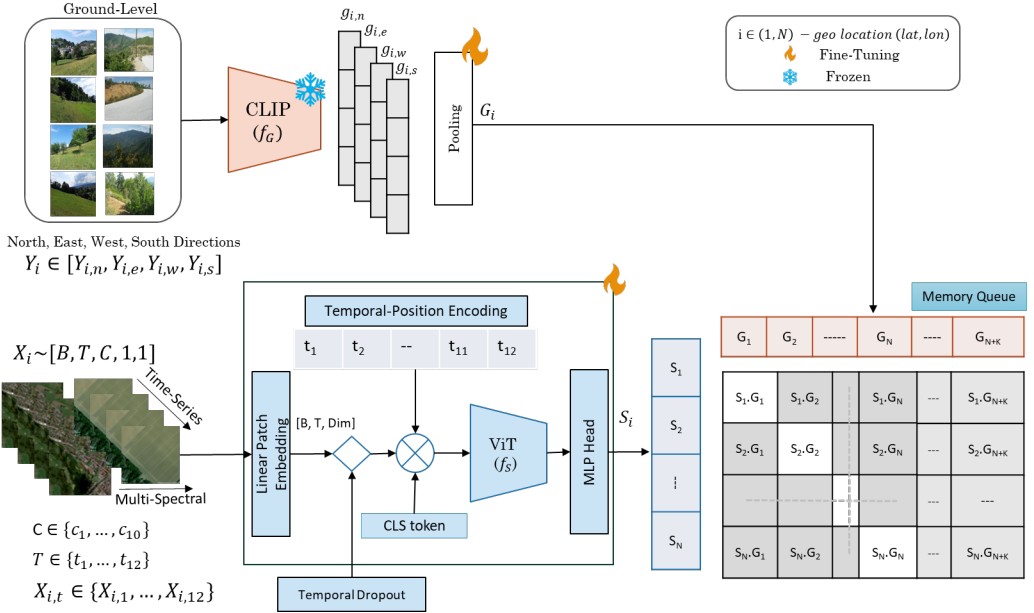


Figure 2. TimeSenCLIP Model: Spectral-temporal patches from Sentinel-2 are aligned with ground-level CLIP features using contrastive learning. The satellite encoder learns from minimal spatial input via a ViT, while a memory queue enables efficient negative sampling.

multi-temporal Sentinel-2 observations aligned with LUCAS (2018) locations. The dataset contains non-overlapping  $64 \times 64$  pixel patches, each with annual composite imagery across 10 spectral bands. The dataset has splits training (140k), validation (30k), and test sets (50k), with no location overlap. We extract fixed-size patches (e.g.,  $1 \times 1$ ,  $5 \times 5$  and  $9 \times 9$ ) for satellite encoding, varying them during ablation.

#### 4. Experimental Setup

##### 4.1 Implementation Details

Our implementation of TimeSenCLIP consists of two components: a frozen ground-level image encoder and a trainable satellite image time-series encoder, trained using contrastive learning.

For the ground encoder, we use the ViT-B/32 CLIP model pre-trained on natural images, applied to the four LUCAS directional ground-level photos (north, east, south, west) per site. Each image is passed through the frozen CLIP encoder, and the resulting features are combined via attention pooling. This yields a single ground-level feature vector per location.

The satellite encoder receives single-pixel multispectral time-series from Sentinel-2, formatted as sequences of shape  $T \times C$  (temporal steps  $\times$  spectral bands). Each timestep of the time series is embedded via a linear layer, and learnable temporal positional embeddings are added. An additional ‘‘class token’’ is prepended before passing the sequence through a 6-layer Transformer (8 heads, 512 hidden dimension, 256 latent size), using GELU activation function and LayerNorm. A lightweight MLP head projects the time token output to the shared embedding space.

**Temporal-Spectral Augmentation Strategies** To account for the missing values commonly encountered in time series from satellite observations due to factors like cloud cover, seasonal occlusions, or data quality issues, we apply stochastic

temporal dropout during training. With a 50% probability, we trained three models with the following augmentation strategies:

- **Random TSDrop:** Random time steps are independently masked to simulate irregular or missing observations across the temporal sequence. This ranged between 1 to 11 time steps masking.

- **TSMixAug:** This strategy utilises two complementary forms of temporal augmentation, each applied with a 50% probability:

- Random Quarterly Masking (25%): We randomly select and mask a contiguous block of three months (i.e., one quarter) from the input sequence to simulate partial temporal data.

- Median Pooling (25%): The full temporal sequence is collapsed into a single vector by computing the median across time steps, reducing temporal variability.

- **TSMSDrop:** Both the temporal and spectral dimensions are randomly masked to simulate scenarios like multi-modal degradation or sensor failures. For spectral dropout, the RGB bands are always kept, while the remaining spectral bands are randomly removed. Similarly, timestamps in the temporal sequence are also randomly dropped.

These augmentation strategies encourage the model to remain robust under incomplete or aggregated temporal signals.

Training is performed using the AdamW optimizer with an initial learning rate of  $10^{-4}$ , a cosine annealing schedule, and 10 warm-up epochs. All experiments are conducted on a single NVIDIA TITAN X GPU.

## 4.2 Evaluation Tasks and Datasets

We evaluate TimeSenCLIP across a suite of geo-referenced prediction tasks spanning land classification, ecosystem mapping, and visual perception benchmarks.

**Land Use / Land Cover and Crop Type** We use coarse-grained land use and land cover (LULC) labels derived from the CORINE classification, including categories such as artificial surfaces, croplands, grasslands, wetlands and forest. These labels are sourced from the LUCAS field survey<sup>1</sup> conducted across Europe and define a multi-class classification task with 10–15 categories based on real-world observations. The Level 0 taxonomy includes 8 land cover and 18 land use classes, while Level 1 refines cropland into 36 specific crop types.

**Biogeographical Zones** (European Environment Agency, 2016): This dataset stratifies Europe into 11 distinct ecological regions (e.g., Alpine, Boreal, Mediterranean) based on climate, topography, and vegetation. Each LUCAS location is mapped to its corresponding ecological zone. Of the 11 bioregions, Arctic, Anatolian, Macaronesian, and Outside were excluded as they were not represented in the LUCAS geo-tags.

**EUNIS Habitat Classes** (European Environment Agency, 2019): We leverage Level 2 of the EUNIS classification hierarchy, consisting of 44 habitat types (e.g., “Mixed deciduous and coniferous woodland”, “Arable land and market gardens”). These finer-grained labels provide a more detailed ecological understanding, complementing land use annotations.

**Scenicness Prediction** This task is formulated as a visual regression problem aimed at predicting the perceived beauty of landscapes (Workman et al., 2017, Levering et al., 2021, Levering et al., 2024). We utilize the ScenicOrNot (SoN) dataset (Seresinhe et al., 2015), which contains geotagged images across the United Kingdom rated by human annotators on a scale from 1 to 10. These crowd-sourced ratings represent subjective visual preferences and serve as ground truth for evaluating aesthetic perception. To further explore this task, we build on the work of Levering et al. (Levering et al., 2024), which introduced scenicness-oriented textual prompts (e.g., “a busy highway” vs. “a mountain”) and measured human preferences across them. Inspired by their approach, we evaluate our model using the same prompts and apply late prompt ensembling to better capture concept-level scenicness. The evaluation are done on 2,411 Sen4Map image samples from the United Kingdom (UK), paired with SoN dataset scores and aligned to both LUCAS/Sen4Ma and SoN locations, to incorporate temporal and spectral dimensions.

Together, these datasets enable comprehensive evaluation of the model’s capacity for landscape characterization, capturing both LULC patterns and broader ecological attributes across diverse European regions.

## 4.3 Evaluation Setup

**Prompt Design** For the zero-shot evaluation, we use three types of textual prompts: (i) class names, (ii) templated prompts of the form “a centered satellite image of {class}”, and (iii) descriptive texts. Five descriptive prompts for each class were generated using OpenAI GPT-4, following a prompt style similar to that used in SenCLIP (Jain et al., 2025). Examples of these descriptive prompts are provided in Table 1.

<sup>1</sup> <https://ec.europa.eu/eurostat/documents/205002/8072634/LUCAS2018-C3-Classification.pdf#page=10.09>

**Temporal Aggregation** In addition, we evaluate the model under three temporal aggregation strategies. The monthly setting uses all 12 individual time steps. The quarterly setting reduces the sequence to 4 time steps, each computed as the median of a 3-month window. The annual (Single) setting further compresses the sequence to a single representation by taking the median across all 12 months.

We compared TimeSenCLIP with baseline models including CLIP (Radford et al., 2021), GeoRSCLIP (Zhang et al., 2023), RemoteCLIP (Liu et al., 2023), SkyCLIP (Wang et al., 2024), and SenCLIP (Jain et al., 2025). All baseline models used fixed  $64 \times 64$  patches resized to  $224 \times 224$ , emphasizing spatial patterns. In contrast, TimeSenCLIP operates directly on single pixel inputs.

## 5. Results and Discussion

### 5.1 Zeroshot Results

We evaluate top-1 zero-shot classification accuracy across five geospatial tasks: Land Cover (LC), Land Use (LU), EUNIS habitat types, Bioregions, and crop types. The results are summarized in Table 2. Notably, even with single-temporal and single-pixel input, TimeSenCLIP consistently outperforms spatial and RGB image based baselines such as CLIP, SenCLIP, and GeoRSCLIP. This highlights the strong discriminative capacity of its multi-spectral encoding, demonstrating that spectral diversity alone without spatial context can yield robust performance, making it a crucial factor in remote sensing tasks.

Incorporating temporal information through monthly and quarterly time slices delivers further performance gains, with the Random TSDrop variant achieving the highest scores in several categories, including 66.07% on Land Cover and 41.11% on Crops. Other temporal dropout methods also show strong robustness across task types, with TSMixAug and TSMSDrop delivering competitive accuracy.

We also observe that as TimeSenCLIP trained with ground-level imagery benefit from more descriptive prompts framed from a ground-level perspective, yielding consistent improvements in most tasks. The only exception is Bioregions, where simpler prompts using just class names perform best.

These results highlight the strength of contrastive learning over spectral-temporal inputs, which enables the model to capture seasonal dynamics and time-dependent cues relevant for remote sensing tasks.

### 5.2 Image-To-Image Retrieval Tasks

Table 3 presents the image-to-image retrieval performance across Satellite-to-Ground (S2G) and Ground-to-Satellite (G2S) directions, evaluated under three temporal configurations: Single, Quarterly, and Monthly. The evaluation spans a broad range of semantic categories, including LULC, EUNIS habitat types, biogeographical regions, crop types, and country-level classifications. The primary metric used is Recall@1. Across all configurations and categories, our proposed TimeSenCLIP variants outperform existing baseline models such as CLIP, GeoRSCLIP, RemoteCLIP, SkyCLIP, and SenCLIP. These improvements reflect the effectiveness of incorporating temporal dynamics and the proposed dropout strategies in enhancing satellite-ground image alignment.

| Category                                  | Descriptive Prompts  |
|---|--|
| Sparsely wooded grasslands (EUNIS)        | Sparse canopy with open fields; scattered trees on grass; visible bare ground between patches. |
| Seasonally wet and wet grasslands (EUNIS) | Wet meadows with reflective surfaces; dark wet zones amid dry land; green patches with water.  |
| Boreal (Bio-Region)                       | Dense pine and spruce forests; mossy forest floors in coniferous areas.                        |
| Mediterranean (Bio-Region)                | Olive/vineyard rows on slopes; dry, dusty terrain with sparse summer vegetation.               |
| Common Wheat (Crops)                      | Wheat fields near harvest; thriving wheat across Europe.                                       |
| Olive Groves (Crops)                      | Mediterranean olives, oil and pickles.; traditional olive landscapes in Greece, Italy, Spain.  |
| Scenicness                                | Wide motorway; busy highway; misty mountain lake; grassy bog surrounded by hills.              |

Table 1. Examples of descriptive prompts, together with their associated category.

| Model                      | Temporal  | Land Cover   |              |              | Land Use     |              |              | EUNIS        |              |              | Bio Regions  |              |              | Crops        |              |              |
|----------------------------|-----------|--------------|--------------|--------------|--------------|--------------|--------------|--------------|--------------|--------------|--------------|--------------|--------------|--------------|--------------|--------------|
|                            |           | Class        | Gen          | Desc         |
| Supervised Upper Bound     | Single    | 63.92        | -            | -            | 66.93        | -            | -            | 49.28        | -            | -            | 42.74        | -            | -            | 29.50        | -            | -            |
| Supervised Upper Bound     | Quarterly | 74.84        | -            | -            | 76.00        | -            | -            | 57.07        | -            | -            | 65.83        | -            | -            | 53.84        | -            | -            |
| Supervised Upper Bound     | Monthly   | 78.65        | -            | -            | 79.30        | -            | -            | 60.52        | -            | -            | 85.39        | -            | -            | 64.60        | -            | -            |
| CLIP                       | Single    | 30.05        | 32.38        | 40.02        | 40.19        | 47.20        | 34.76        | 12.71        | 18.05        | 20.58        | 16.79        | 16.80        | 17.44        | 3.05         | 2.61         | 4.41         |
| GeoRSCLIP                  | Single    | 35.20        | 37.70        | 42.35        | 35.56        | 51.58        | 49.35        | 13.99        | 24.82        | 26.35        | 19.70        | 21.51        | 18.12        | 3.18         | 4.63         | 3.58         |
| RemoteCLIP                 | Single    | 28.43        | 39.60        | 37.13        | 39.26        | 41.69        | 41.86        | 13.58        | 13.29        | 16.74        | 16.47        | 19.17        | 15.63        | 2.35         | 5.80         | 2.29         |
| SkyCLIP                    | Single    | 22.45        | 25.31        | 35.17        | 3.80         | 4.72         | 27.64        | 2.75         | 2.97         | 4.01         | 9.26         | 21.23        | 15.06        | 2.14         | 2.32         | 3.44         |
| SenCLIP                    | Single    | 38.11        | 39.08        | 42.25        | 32.04        | 30.06        | 37.69        | 26.61        | 22.33        | 22.37        | <b>29.45</b> | <b>33.80</b> | 20.71        | 3.40         | 3.54         | 4.63         |
| TimeSenCLIP* Random TSDrop | Single    | 54.46        | 54.22        | 56.17        | 49.61        | 51.03        | 59.68        | 28.76        | 25.05        | 25.52        | 28.50        | 25.05        | <b>24.55</b> | 7.75         | 8.09         | 12.22        |
| TimeSenCLIP TSMSDrop       | Single    | 53.73        | 53.12        | 55.08        | <b>52.63</b> | 52.53        | 58.63        | 27.81        | <b>26.82</b> | <b>27.38</b> | 24.97        | 26.82        | 22.11        | 6.53         | 6.62         | 9.87         |
| TimeSenCLIP TSMixAug       | Single    | <b>55.03</b> | <b>55.45</b> | <b>56.42</b> | 50.29        | <b>54.57</b> | <b>60.26</b> | <b>30.14</b> | 26.00        | 26.29        | 26.29        | 26.00        | 23.81        | <b>10.23</b> | <b>9.30</b>  | <b>18.86</b> |
| TimeSenCLIP Random TSDrop  | Quarterly | 60.61        | 58.93        | <b>63.68</b> | 52.73        | 53.87        | <b>63.98</b> | 27.38        | 27.36        | 30.33        | <b>35.00</b> | 27.36        | <b>25.54</b> | 24.00        | 22.97        | 35.99        |
| TimeSenCLIP TSMSDrop       | Quarterly | <b>61.76</b> | <b>59.56</b> | 63.18        | <b>53.18</b> | 54.23        | 63.47        | <b>31.18</b> | 28.25        | <b>31.67</b> | 34.46        | 28.25        | 25.52        | 24.41        | 22.93        | 33.84        |
| TimeSenCLIP TSMixAug       | Quarterly | 60.80        | 59.42        | 63.15        | 52.98        | <b>54.68</b> | 62.92        | 30.22        | <b>29.65</b> | 31.33        | 32.80        | <b>29.65</b> | 23.90        | <b>24.97</b> | <b>24.05</b> | <b>36.81</b> |
| TimeSenCLIP Random TSDrop  | Monthly   | 63.25        | 61.67        | <b>66.07</b> | <b>54.97</b> | 56.06        | 64.38        | <b>28.52</b> | <b>29.62</b> | <b>33.46</b> | 38.14        | <b>29.62</b> | 24.79        | 28.51        | 28.03        | <b>41.11</b> |
| TimeSenCLIP TSMSDrop       | Monthly   | 61.76        | 60.31        | 64.93        | 53.80        | 53.81        | 64.36        | 22.37        | 22.91        | 30.32        | 39.61        | 22.91        | <b>27.43</b> | <b>30.84</b> | 28.44        | 38.09        |
| TimeSenCLIP TSMixAug       | Monthly   | <b>63.40</b> | <b>61.71</b> | 65.54        | 54.76        | <b>56.33</b> | <b>65.04</b> | 27.88        | 25.88        | 32.23        | <b>39.80</b> | 25.88        | 27.07        | 30.75        | <b>31.38</b> | 40.97        |

Table 2. Top-1 zero-shot accuracy (%) for Land Cover, Land Use, EUNIS, Bio Region, and Crops classification tasks. The “Supervised upper bound” reports TimeSenCLIP encoder results using single pixel inputs with their respective class labels, while the remaining rows present zero-shot performance comparisons between baseline models and TimeSenCLIP. \* Baseline models (CLIP, GeoRSCLIP, RemoteCLIP, SkyCLIP, and SenCLIP) use 64x64-pixel inputs, whereas TimeSenCLIP operates on a single pixel. The best score within each temporal setting is shown in **bold**, and the overall best score in **bold-underline**.

Baseline models that do not incorporate temporal aggregation consistently, underperforms in retrieval tasks, especially in temporally dynamic categories such as Crops and Country, where seasonal variation and phenological cycles are critical for correct class differentiation. While GeoRSCLIP shows competitive results in categories like Land Use and Biogeographical Regions, attributable to its inclusion of Sentinel-2 during training, it underperforms in fine-grained categories that demand temporal specificity. Furthermore, we observe that retrieval from G2S consistently outperforms S2G, likely due to the higher variability and ambiguity in ground-level images, which makes it more difficult for the model to localize the correct match starting from satellite imagery.

Temporal aggregation significantly boosts retrieval accuracy across most categories. Monthly and Quarterly aggregation, in particular, outperform single-temporal baselines by capturing seasonal and intra-annual patterns. Among the TimeSenCLIP variants, those employing Random TSDrop and TSMixAug exhibit the most consistent gains. TSMixAug performs strongly in tasks like EUNIS and Biogeographical Regions, while Random TSDrop yields superior results in temporally dynamic classes such as Crops and Country, especially in the S2G direction. TSMSDrop, which jointly drops spectral and temporal dimensions, also contributes positively, though it slightly lags behind the other two dropout schemes. These findings collectively validate the effectiveness of temporal modeling, dropout regularization, and adaptive fusion strategies for cross-view representation learning.

### 5.3 Scenicness with Prompt Ensembling

Table 4. presents a comprehensive comparison of different prompt ensembling strategies (Levering et al., 2024) applied to scenicness prediction on United Kingdom locations, evaluated using Pearson’s  $R$  and Kendall’s  $\tau$  correlations. All models are assessed with single-temporal input, while TimeSenCLIP variants are additionally tested with quarterly and monthly ensembling using early fusion and multi-prompt averaging across 2, 5, 8, and 10 prompts.

Under single-temporal input, CLIP achieves the highest average performance ( $R = 0.517$ ,  $\tau = 0.362$ ), confirming its strong baseline for aesthetic alignment in static settings. GeoRSCLIP and RemoteCLIP follow, though with reduced performance on temporally-sensitive cues. Among TimeSenCLIP variants, the introduction of temporal dropout (e.g., Random TSDrop and TSMSDrop) initially results in lower scores ( $R = 0.322$  and  $0.271$ , respectively), for single temporal settings.

However, as temporal ensembling is introduced, a marked improvement is observed across all TimeSenCLIP variants. Quarterly ensembling with TSMixAug shows substantial gains, peaking at  $R = 0.473$  and  $\tau = 0.328$ , highlighting the benefit of aligning seasonal dropout patterns with temporal semantic abstraction. The best results are achieved with monthly prompt ensembling, where Random TSDrop outperforms all models ( $R = 0.526$ ,  $\tau = 0.363$ ). This demonstrates the effectiveness of fine-grained temporal modeling and prompt diversity in capturing nuanced aesthetic cues. Both TSMixAug and TSMSDrop also benefit from monthly ensembling, but consistently fall short of Random TSDrop, underscoring the robustness and adaptability

| Model                     | Temporal  | Land Cover   |              | Land Use     |              | EUNIS        |              | Bio Regions  |              | Crops        |              | Country      |              |
|---------------------------|-----------|--------------|--------------|--------------|--------------|--------------|--------------|--------------|--------------|--------------|--------------|--------------|--------------|
|                           |           | G2S          | S2G          |
| CLIP                      | Single    | 0.438        | 0.141        | 0.513        | 0.152        | 0.360        | 0.269        | 0.361        | 0.231        | 0.157        | 0.127        | 0.130        | 0.047        |
| GeoRSCLIP                 | Single    | 0.439        | 0.313        | <b>0.628</b> | 0.274        | <b>0.386</b> | 0.241        | <b>0.425</b> | 0.263        | 0.165        | 0.087        | 0.116        | 0.077        |
| RemoteCLIP                | Single    | 0.394        | 0.406        | 0.539        | 0.496        | 0.368        | 0.188        | 0.283        | 0.200        | 0.060        | 0.078        | 0.099        | 0.025        |
| SkyCLIP                   | Single    | 0.114        | 0.305        | 0.257        | 0.255        | 0.064        | 0.121        | 0.221        | 0.242        | 0.025        | 0.030        | 0.075        | 0.049        |
| SenCLIP                   | Single    | 0.460        | 0.412        | 0.501        | 0.446        | 0.343        | 0.253        | 0.414        | 0.461        | 0.111        | 0.079        | <b>0.167</b> | <b>0.190</b> |
| TimeSenCLIP Random TSDrop | Single    | <b>0.560</b> | <b>0.557</b> | 0.594        | 0.550        | 0.360        | 0.347        | 0.357        | 0.363        | <b>0.188</b> | 0.142        | 0.160        | 0.162        |
| TimeSenCLIP TSMSDrop      | Single    | 0.477        | 0.541        | 0.591        | 0.524        | 0.307        | 0.330        | 0.375        | 0.368        | 0.179        | 0.123        | 0.154        | 0.171        |
| TimeSenCLIP TSMixAug      | Single    | 0.529        | 0.550        | 0.608        | <b>0.565</b> | 0.362        | <b>0.349</b> | 0.356        | 0.390        | 0.134        | <b>0.160</b> | 0.158        | 0.157        |
| TimeSenCLIP Random TSDrop | Quarterly | 0.592        | 0.648        | 0.623        | <b>0.663</b> | 0.388        | 0.414        | 0.447        | 0.537        | 0.244        | <b>0.357</b> | 0.215        | 0.300        |
| TimeSenCLIP TSMSDrop      | Quarterly | <b>0.612</b> | 0.676        | 0.615        | 0.654        | 0.376        | 0.405        | 0.501        | 0.551        | <b>0.248</b> | 0.325        | 0.229        | 0.328        |
| TimeSenCLIP TSMixAug      | Quarterly | 0.611        | <b>0.683</b> | <b>0.633</b> | 0.651        | <b>0.401</b> | <b>0.415</b> | <b>0.507</b> | <b>0.581</b> | 0.233        | 0.344        | <b>0.262</b> | <b>0.358</b> |
| TimeSenCLIP Random TSDrop | Monthly   | <b>0.607</b> | 0.659        | <b>0.637</b> | <b>0.690</b> | 0.398        | 0.436        | <b>0.544</b> | <b>0.648</b> | <b>0.293</b> | <b>0.433</b> | <b>0.295</b> | <b>0.415</b> |
| TimeSenCLIP TSMSDrop      | Monthly   | 0.578        | <b>0.660</b> | 0.613        | 0.686        | 0.383        | 0.429        | 0.492        | 0.597        | 0.215        | 0.388        | 0.230        | 0.306        |
| TimeSenCLIP TSMixAug      | Monthly   | 0.605        | 0.648        | 0.621        | 0.684        | <b>0.408</b> | <b>0.441</b> | 0.506        | 0.618        | 0.193        | 0.408        | 0.258        | 0.337        |

Table 3. Image-to-Image Retrieval performance for Satellite-to-Ground (S2G) and Ground-to-Satellite (G2S) tasks, evaluated across multiple temporal settings (Single, Quarterly, Monthly) with recall@1 used as the primary metric. **Bold** values represent the best performance within each temporal setting, while **bold-underline** values indicate the overall best recall across all settings and models, highlighting the most effective temporal strategy for each task.

| Model                                     | Temporal  | Early        |              | 2            |              | 5            |              | 8            |              | 10           |              | Average      |              |
|---|-----------|--------------|--------------|--------------|--------------|--------------|--------------|--------------|--------------|--------------|--------------|--------------|--------------|
|   |           | R            | Tau          |
| CLIP (SON Images) (Levering et al., 2024) | Single    | 0.544        | 0.390        | 0.692        | 0.485        | 0.654        | 0.447        | 0.673        | 0.479        | 0.623        | 0.450        | 0.637        | 0.450        |
| CLIP                                      | Single    | 0.510        | 0.358        | <b>0.547</b> | <b>0.384</b> | 0.547        | <b>0.384</b> | <b>0.536</b> | <b>0.379</b> | 0.444        | 0.307        | 0.517        | 0.362        |
| GeoRSCLIP                                 | Single    | 0.478        | 0.346        | 0.520        | 0.378        | 0.512        | 0.369        | 0.466        | 0.336        | 0.306        | 0.212        | 0.456        | 0.328        |
| RemoteCLIP                                | Single    | 0.435        | 0.295        | 0.477        | 0.321        | 0.473        | 0.318        | 0.478        | 0.325        | 0.397        | 0.260        | 0.452        | 0.304        |
| SkyCLIP                                   | Single    | 0.365        | 0.249        | 0.207        | 0.124        | 0.246        | 0.154        | 0.245        | 0.153        | 0.391        | 0.255        | 0.291        | 0.187        |
| SenCLIP                                   | Single    | 0.396        | 0.272        | 0.459        | 0.310        | 0.440        | 0.297        | 0.420        | 0.286        | 0.366        | 0.241        | 0.416        | 0.281        |
| TimeSenCLIP Random TSDrop                 | Single    | 0.336        | 0.223        | 0.345        | 0.231        | 0.346        | 0.231        | 0.308        | 0.200        | 0.274        | 0.167        | 0.322        | 0.210        |
| TimeSenCLIP TSMSDrop                      | Single    | 0.305        | 0.209        | 0.300        | 0.200        | 0.300        | 0.208        | 0.250        | 0.167        | 0.200        | 0.128        | 0.271        | 0.182        |
| TimeSenCLIP TSMixAug                      | Single    | 0.382        | 0.254        | 0.394        | 0.263        | 0.389        | 0.261        | 0.347        | 0.235        | 0.294        | 0.186        | 0.361        | 0.240        |
| TimeSenCLIP Random TSDrop                 | Quarterly | 0.438        | 0.309        | 0.479        | 0.324        | 0.468        | 0.325        | <b>0.445</b> | 0.313        | 0.413        | 0.288        | 0.449        | 0.312        |
| TimeSenCLIP TSMSDrop                      | Quarterly | 0.443        | 0.305        | 0.458        | 0.303        | 0.451        | 0.310        | 0.419        | 0.300        | 0.375        | 0.262        | 0.429        | 0.296        |
| TimeSenCLIP TSMixAug                      | Quarterly | 0.464        | 0.327        | 0.505        | 0.338        | 0.493        | 0.340        | 0.470        | 0.331        | 0.435        | 0.305        | 0.473        | 0.328        |
| TimeSenCLIP Random TSDrop                 | Monthly   | <b>0.518</b> | <b>0.361</b> | <b>0.558</b> | 0.371        | <b>0.548</b> | 0.373        | 0.526        | 0.366        | <b>0.478</b> | <b>0.343</b> | <b>0.526</b> | <b>0.363</b> |
| TimeSenCLIP TSMSDrop                      | Monthly   | 0.488        | 0.342        | 0.519        | 0.343        | 0.510        | 0.350        | 0.478        | 0.343        | 0.420        | 0.309        | 0.483        | 0.337        |
| TimeSenCLIP TSMixAug                      | Monthly   | 0.499        | 0.351        | 0.550        | 0.365        | 0.535        | 0.367        | 0.511        | 0.359        | 0.463        | 0.333        | 0.512        | 0.355        |

Table 4. Scenicness estimation on UK data points: R and Kendall’s Tau scores for various models evaluated under different prompt ensembling strategies (as proposed by Levering et al., 2024) across Single, Quarterly, and Monthly temporal resolutions. While Levering et al. focused on ground-level images (scenic vs. non-scenic) using CLIP ViT-L/14, we extend the analysis to Sentinel-2 satellite imagery, achieving competitive performance on a smaller dataset using the lightweight ViT-B/32 text encoder.

of randomized temporal dropout when integrated with detailed temporal semantic aggregation.

While CLIP demonstrates strong performance even with single-temporal images, our results show that TimeSenCLIP achieves competitive performance using only single pixel inputs, particularly when enriched with temporal context. The gains from quarterly and monthly ensembling underscore TimeSenCLIP’s strength in leveraging temporal dynamics, enabling it to model seasonal patterns and nuanced landscape features more effectively despite its minimal spatial footprint.

#### 5.4 Ablation Study

##### 5.4.1 Spatial Context

**Zeroshot** Remarkably, TimeSenCLIP with single pixel consistently outperforms spatially-aware baselines like CLIP and GeoRSCLIP (using 64×64 patches), demonstrating the superior discriminative power of temporally-resolved spectral features when optimized through contrastive pretraining.

To systematically evaluate spatial influence, we extended TimeSenCLIP to process 5×5 and 9×9 patches (Figure 3). Our

analysis reveals that while 5×5 patches occasionally yield marginal improvements (e.g., +4.3% in Land Cover tasks), 9×9 patches typically degrade performance. This effect is especially evident in crop type classification, where expanded spatial context (e.g., using 5×5 or 9×9 patches) does not improve accuracy and can even reduce it. While these larger patches still retain temporal information, the added spatial context introduces noise from heterogeneous neighboring pixels. This suggests that for crop classification, the key discriminative features lie in the temporal and spectral signatures associated with crop phenology, and the additional spatial context does not contribute meaningful information, instead, it may dilute the signal.

These results establish that for zero-shot geospatial classification, high-resolution spectral-temporal learning provides more critical discriminative signals than broader spatial context. The performance degradation observed with larger patches suggests an inherent tradeoff: while minimal spatial context (5×5) can occasionally help, the spectral-temporal domain remains the dominant factor for optimal performance.

**Image-To-Image Retrieval** Figure 4 presents the influence of spatial patch size in image-to-image retrieval performance across various tasks. Unlike zero-shot classification, where

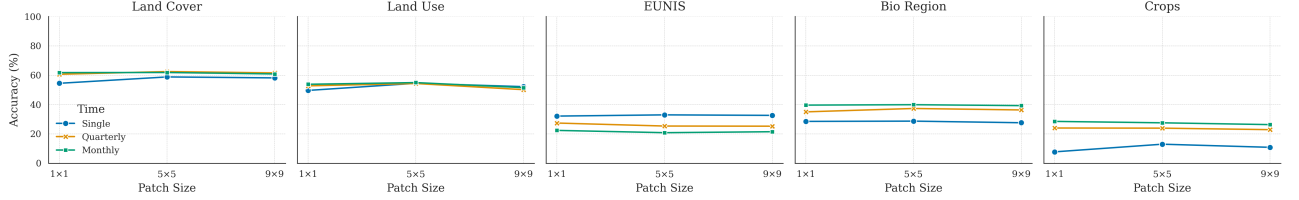


Figure 3. Impact of Spatial Information on Zeroshot Classification Top-1 Accuracy (%) for Different Mapping Tasks

moderate spatial context yields limited gains up to a point, retrieval performance is more task-specific and directionally asymmetric.

For EUNIS, BioRegion, and Country, increasing the spatial patch size from 1x1 to 5x5 and 9x9 consistently improves retrieval performance in both S2G and G2S directions. These tasks represent spatially coherent or regionally structured classes, where neighboring context enhances semantic alignment during retrieval.

In contrast, for Land Cover, Land Use, and Crop types, the benefit of larger patches is limited or inconsistent. S2G retrieval can see moderate gains from increased context, but G2S performance often declines with larger patches. This suggests that excessive spatial aggregation may introduce noise or blur discriminative details, particularly in spatially heterogeneous or spectrally sensitive categories.

At the Single temporal resolution, increasing patch size can deliver substantial gains, e.g., Land Use S2G jumps by +10.10 points from 1x1 to 5x5. However, as temporal resolution increases to Monthly, the extra benefit from spatial context largely disappears, with differences between 1x1 and 5x5 often within 1–2 points (e.g., Land Cover G2S: 60.70 % vs. 61.40 %; Bio Region S2G: 64.80 % vs. 65.60 %). This suggests that rich temporal information already captures much of the variation that broader spatial context would otherwise provide.

This pattern highlights that while temporal aggregation strengthens retrieval across all patch sizes, spatial context changes have a more pronounced effect in low-temporal settings and for spatially coherent classes, whereas for high-temporal settings, smaller patches already capture most of the relevant information.

**5.4.2 Impact of Dropout Strategies** To assess the robustness and generalization ability of our model, we perform an ablation study using spectral and temporal dropout, where a random subset of spectral bands or timestamps is dropped during training. This strategy simulates missing or noisy observations and encourages the model to rely on more stable and discriminative patterns. Table 5 reports the impact on zero-shot classification, and Table 6 on image-to-image retrieval.

**Zero-Shot Classification.** Table 5 shows that temporal dropout (TS Drop) has a clearly positive effect across all tasks. The no-dropout baseline provides balanced but moderate performance, e.g., 50.16% on Land Cover and 45.94% on Land Use, with lower accuracy on more challenging categories like EUNIS (20.60%) and Crops (17.06%). This setting reflects the model’s raw capacity without additional regularization.

Adding temporal dropout alone delivers the most consistent and substantial gains, improving Land Cover by +10.4% and Land

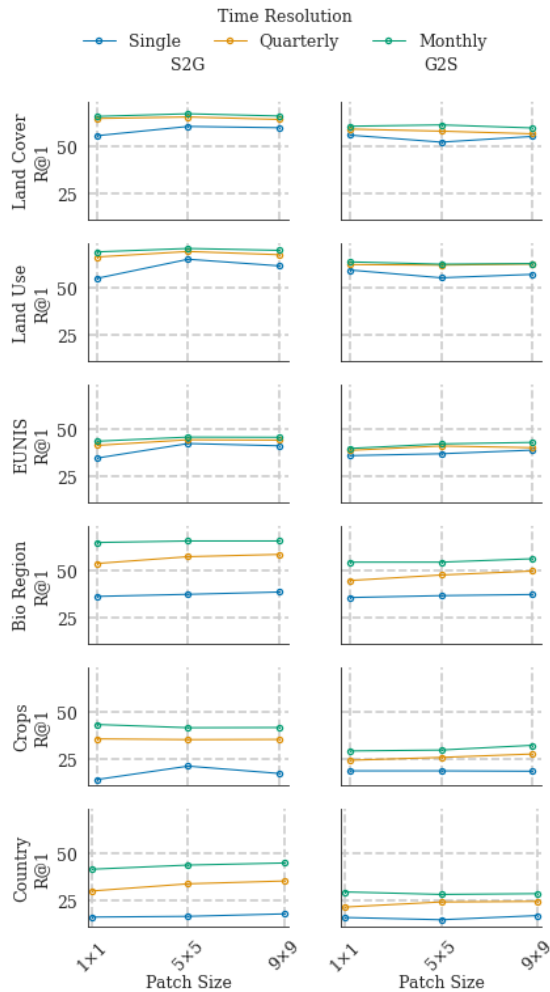


Figure 4. Impact of Spatial Information on Image-to-Image Retrieval for Satellite-to-Ground (S2G) and Ground-to-Satellite (G2S) tasks across Different Ecological Mappings.

| MS Drop | TS Drop | Land Cover   | Land Use     | EUNIS        | Bioregion    | Crops        |
|---------|---------|--------------|--------------|--------------|--------------|--------------|
| ✗       | ✗       | 50.16        | 45.94        | 20.60        | 31.07        | 17.06        |
| ✓       | ✗       | 48.11        | 45.43        | 20.83        | 30.47        | 16.69        |
| ✗       | ✓       | <b>60.60</b> | <b>58.41</b> | 28.39        | <b>33.52</b> | <b>21.56</b> |
| ✓       | ✓       | 58.53        | 57.97        | <b>29.71</b> | 31.97        | 20.34        |

Table 5. Effect of Multispectral (MS) and Temporal (TS) Dropout on Zero-Shot Performance (Top-1 Accuracy %). The table reports average Top-1 accuracy across different prompts and temporal settings. (✓) indicates dropout is applied, (✗) otherwise.

Use by +12.5% over the baseline. These gains indicate that introducing randomness in the temporal axis during training helps the model learn features that are robust to temporal inconsistencies, such as seasonal shifts or missing acquisitions, which are common in satellite imagery.

In contrast, spectral dropout (MS Drop) shows a more nuanced impact. When applied alone, it causes declines in performance across most tasks (e.g., -2.0% on Land Cover, -0.6% on Bioregion). This indicates that randomly dropping spectral bands can hinder learning, especially for tasks that rely on subtle spectral cues for fine-grained class distinctions. These findings reinforce our earlier results in Table 2, where TimeSenCLIP, even when restricted to single-temporal and single-pixel input, outperformed RGB-based and spatial baselines, highlighting the critical role of multi-spectral information in driving strong performance.

When both spectral and temporal dropout are applied together, the results are mixed. In some tasks like EUNIS, this dual dropout leads to the highest accuracy (29.71%), possibly because it forces the model to learn more invariant representations across both axes. However, in others like Land Cover and Crops, performance is slightly worse than using temporal dropout alone. This suggests that while combined dropout introduces helpful regularization, it can also suppress informative signals when the input becomes too sparse or noisy.

**Image-to-Image Retrieval.** The trends observed in zero-shot classification largely hold for retrieval as well (Table 6). Temporal dropout alone consistently improves Recall@1 across most tasks, especially on Land Cover (+4.1%) and EUNIS (+3.0%), reinforcing the importance of learning temporally robust embeddings. This is particularly valuable in retrieval, where satellite scenes often vary in acquisition dates, lighting, or phenological stage.

| MS Drop | TS Drop | Land Cover   | EUNIS        | Bioregion    | Crops        | Country      |
|---------|---------|--------------|--------------|--------------|--------------|--------------|
| ✗       | ✗       | 56.32        | 36.65        | 46.48        | <b>25.17</b> | 25.30        |
| ✓       | ✗       | 56.27        | 36.83        | 48.80        | 23.83        | <b>27.38</b> |
| ✗       | ✓       | <b>60.43</b> | <b>39.60</b> | <b>49.30</b> | 24.53        | 25.50        |
| ✓       | ✓       | 59.07        | 37.17        | 48.07        | 24.63        | 23.63        |

Table 6. Effect of Multispectral (MS) and Temporal (TS) Dropout on Retrieval performance (Recall@1). The table reports average Recall across S2G-G2S and temporal settings. (✓) indicates dropout is applied, (✗) otherwise.

The effect of spectral dropout in retrieval is more task-dependent. It yields modest improvements over no-dropout in Bioregion (+2.3%) and Country (+2.1%), likely because these tasks contain classes that are less sensitive to specific spectral channels and benefit from a broader regularization effect. However, in others like Crop types or Land Cover, MS dropout slightly reduces retrieval accuracy, hinting that key spectral cues are essential for distinguishing certain land classes.

Applying both dropout types together results in competitive but not always optimal performance. For example, while the dual dropout setting remains strong overall, it slightly underperforms the temporal-only setting on most tasks, likely due to excessive noise or reduced signal fidelity from compound stochasticity.

The results suggest that temporal variation is a more critical dimension of resilience in remote sensing models, and selective dropout on the temporal axis during training offers a strong trade-off between robustness and discriminative power, particularly in zero-shot and cross-domain retrieval settings.

## 5.5 Qualitative Analysis

**5.5.1 Scenicness** To better understand the spatial distribution of scenicness predictions, we visualized the model outputs on a map of the UK. Figure 5 shows a side-by-side comparison of the ground truth scenicness scores and the predictions from various model variants, highlighting both consistent patterns and subtle differences across regions. Across all models, a clear trend emerges for urban and densely populated areas, particularly in southern and central England that consistently receive lower scenicness scores, typically shown in magenta or lighter green. In contrast, rural and natural landscapes, especially those in northern England, Scotland, and parts of Wales, are assigned higher scenicness values, represented by darker greens.

While no model perfectly replicates the ground truth, the TimeSenCLIP variants (Single, Quarterly, Monthly) show stronger spatial alignment with the true distribution compared to the baselines. Among them, the Monthly variant stands out for producing smoother spatial gradients and more distinct separation between urban and rural areas, suggesting that multi-temporal information helps capture subtle seasonal and environmental variations. GeoRSCLIP and CLIP also reflect broad spatial trends but tend to underrepresent highly scenic rural clusters and yield more homogenized scores overall. SenCLIP exhibits slightly better differentiation between rural and urban regions but still lacks the finer spatial resolution seen in TimeSenCLIP.

This map-based visualization offers an intuitive lens to assess geographic generalization and further supports our claim that TimeSenCLIP improves spatial sensitivity in scenicness prediction, even if the exact regression to ground truth scores is not fully achieved.

**5.5.2 Text-To-Image Retrieval** Figure 6 presents the quantitative results of text-to-image retrieval, where free-form textual descriptions are used to search for the most semantically relevant satellite image patches. Each query corresponds to a specific land cover, land use, EUNIS habitat class, biogeographic region, or crop type.

Our model, TimeSenCLIP, demonstrates strong performance in matching rich, descriptive text prompts to appropriate satellite imagery, despite the fact that these descriptions are often abstract, high-level, or grounded in human perception (e.g., “traditional olive landscapes in Greece, Italy, Spain.”).

For each text query, we display the Top-5 retrieved satellite patches. These examples showcase the model’s ability to generalize across tasks and semantic levels, from broad biogeographic zones to fine-grained crop types. Retrieved visually

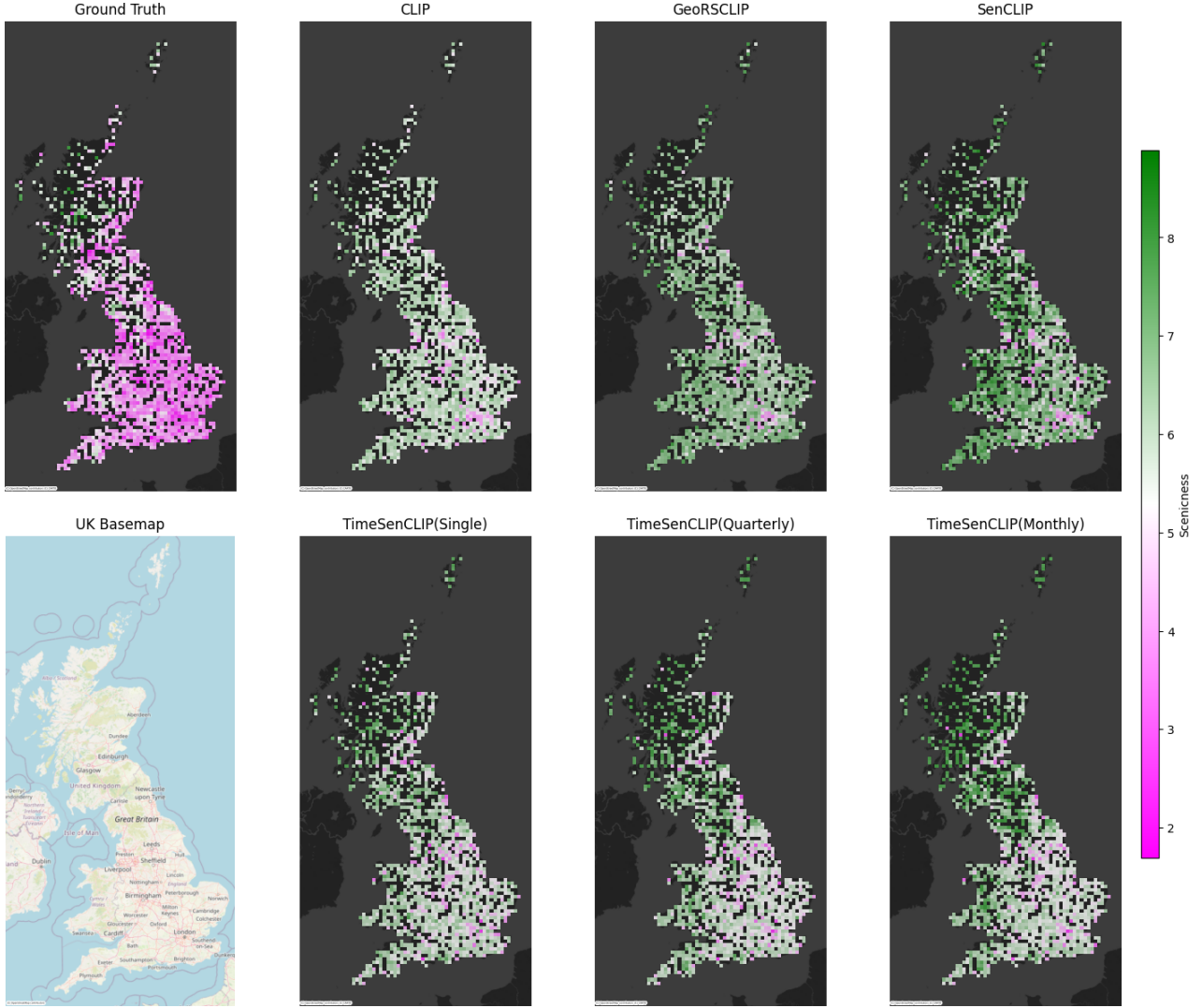


Figure 5. Scenicness scores from 1-10 across UK

and semantically consistent matches, indicating that the learned representation aligns textual semantics with satellite spectral-temporal features effectively.

This experiment demonstrates the practical utility of TimeSenCLIP in real-world scenarios, where users can retrieve relevant satellite imagery using natural language descriptions without relying on predefined class labels. It also underscores the model’s strong zero-shot generalization capabilities, as the textual prompts and categories used during retrieval were not part of the training process. Instead, the model learns to associate semantic meaning through supervision from ground-level imagery, enabling it to match unseen descriptions to appropriate satellite scenes.

### 5.6 Computational Efficiency and Inference Performance

Table 7 highlights the computational efficiency of the proposed TimeSenCLIP model compared to baseline models based on CLIP. Operating on just a single pixel, TimeSenCLIP achieves over 99% reduction in FLOPs and 94% fewer parameters, while being approximately 8x faster at inference and using 63% less GPU memory. Even when spatial patches are expanded to 5x5 or 9x9, the computational cost remains minimal, with only slight increases in memory and latency. This demonstrates that

TimeSenCLIP is highly efficient and well-suited for scalable remote sensing tasks, particularly in resource constrained or real-time settings.

| Model           | FLOPs (GMac) | Parameters (M) | Inference Time (ms) | Peak Memory (MB) |
|-----------------|--------------|----------------|---------------------|------------------|
| CLIP            | 16.690       | 151.28         | 14.14               | 594.13           |
| TimeSenCLIP 1x1 | 0.105        | 8.17           | 1.75                | 219.35           |
| TimeSenCLIP 5x5 | 0.106        | 8.29           | 1.79                | 219.83           |
| TimeSenCLIP 9x9 | 0.110        | 8.58           | 1.88                | 254.53           |

Table 7. Computational Efficiency and Inference Performance Comparison

### 6. Conclusion

This work presents TimeSenCLIP, a temporally and spectrally-aware multimodal framework for zero-shot ecological classification and retrieval. By leveraging fine-grained spectral-temporal inputs and regularization strategies, TimeSenCLIP demonstrates consistent and substantial improvements over existing baselines across diverse remote sensing tasks, including Land Cover, Land Use, EUNIS habitat mapping, Bioregions, Crop types, and Scenicness prediction. Our findings highlight

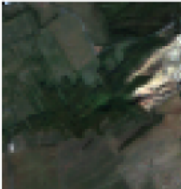
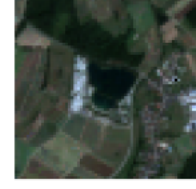
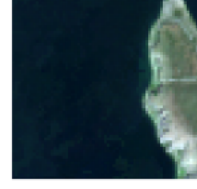
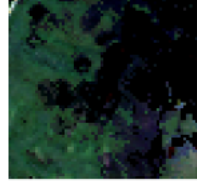
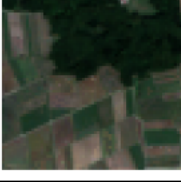
|   |   |  |   |  |  |
|---|---|--|---|--|--|
|  <p>Clear seasonal contrasts are visible with vibrant greens in spring and browns in autumn.</p> | <p>Top Match<br/>Arable land and...<br/>Continental</p>      | <p>Match #2<br/>Broadleaved dec...<br/>Continental</p>      | <p>Match #3<br/>Broadleaved dec...<br/>Atlantic</p>         | <p>Match #4<br/>Broadleaved dec...<br/>Alpine</p>         | <p>Match #5<br/>Broadleaved dec...<br/>Mediterranean</p>    |
|  <p>Mediterranean olives, oil and pickles.</p>   | <p>Top Match<br/>Mediterranean</p>                           | <p>Match #2<br/>Mediterranean</p>                           | <p>Match #3<br/>Mediterranean</p>                           | <p>Match #4<br/>Olive groves<br/>Mediterranean</p>        | <p>Match #5<br/>Mediterranean</p>                           |
|  <p>Shopping centres with glass facades and parked bicycles.</p>                                 | <p>Top Match<br/>Industry and Ma...<br/>Alpine</p>          | <p>Match #2<br/>Industry and Ma...<br/>Atlantic</p>        | <p>Match #3<br/>Commerce, Finan...<br/>Atlantic</p>        | <p>Match #4<br/>Industry and Ma...<br/>Continental</p>   | <p>Match #5<br/>Transport, Comm...<br/>Continental</p>     |
|  <p>Boats moored in quiet harbors at sunset.</p>   | <p>Top Match<br/>Water<br/>Continental</p>                 | <p>Match #2<br/>Water<br/>Atlantic</p>                    | <p>Match #3<br/>Water<br/>Continental</p>                 | <p>Match #4<br/>Water<br/>Mediterranean</p>             | <p>Match #5<br/>Water<br/>Boreal</p>                      |
|  <p>A multi-lane toll plaza with cars lined up during rush hour.</p>                           | <p>Top Match<br/>Transport, Comm...<br/>Mediterranean</p>  | <p>Match #2<br/>Transport, Comm...<br/>Mediterranean</p>  | <p>Match #3<br/>Transport, Comm...<br/>Mediterranean</p>  | <p>Match #4<br/>Semi-natural an...<br/>Continental</p>  | <p>Match #5<br/>Industry and Ma...<br/>Mediterranean</p>  |
|  <p>Maize, biofuel and food.</p>   | <p>Top Match<br/>-<br/>Continental</p>                     | <p>Match #2<br/>Maize<br/>Continental</p>                 | <p>Match #3<br/>Maize<br/>Mediterranean</p>               | <p>Match #4<br/>Common wheat<br/>Continental</p>        | <p>Match #5<br/>-<br/>Mediterranean</p>                   |

Figure 6. Text-to-image retrieval performance using TimeSenCLIP with descriptive prompts. While the model processes single pixel monthly temporal composites during operation, these visualizations show representative RGB 64x64 patches for interpretability. Results demonstrate the system's ability to match textual descriptions with relevant satellite imagery across diverse land cover, land use, bioregions, eunis and crops classes.

the importance of taking into account temporal dynamics particularly at a monthly resolution to capture seasonal and phenological patterns that are critical for fine-grained geospatial understanding.

Ablation studies confirm that temporal dropout enhances robustness to missing or inconsistent observations, while spatial context offers task-specific benefits. Notably, TimeSenCLIP maintains strong performance even when constrained to single pixel inputs, underscoring the power of spectral-temporal learning via contrastive learning. For tasks such as Crop type classification and Scenicness prediction, temporal ensembling and prompt diversification further improve performance, illustrating the value of aligning learned representations with temporal variations.

**Limitations and Future Work** Although our model shows strong performance on ecological tasks in Europe, it has only been evaluated using Sentinel-2 and LUCAS data from the EU. This limits its generalizability to other sensors and regions with different climates, and phenologies. Extending the framework to manage multi-sensor information (e.g. Sentinel-1 and Sentinel-2) and scale up globally, are key directions for possible future works.

### Acknowledgements

This research was supported by the ‘Giving Rural Actors Novel Data and Re-Usable Tools to Lead Public Action in Rural Areas’ (GRANULAR) project, which has received funding from the European Union’s Horizon Europe Research and Innovation Programme under Grant Agreement No. 101061068. This work was also supported in part by the ANR project OB-TEA (ANR-22-CPJ1-0054-01).

### References

Daroya, R., Cole, E., Mac Aodha, O., Van Horn, G., Maji, S., 2024. WildSAT: Learning Satellite Image Representations from Wildlife Observations. *arXiv preprint arXiv:2412.14428*.

Dhakal, A., Ahmad, A., Khanal, S., Sastry, S., Jacobs, N., 2023. Sat2cap: Mapping fine-grained textual descriptions from satellite images. *arXiv preprint arXiv:2307.15904*.

d’Andrimont, R., Yordanov, M., Martinez-Sanchez, L., Eiselt, B., Palmieri, A., Dominici, P., Gallego, J., Reuter, H. I., Joebege, C., Lemoine, G. et al., 2020. Harmonised LUCAS in-situ land cover and use database for field surveys from 2006 to 2018 in the European Union. *Scientific data*, 7(1), 352.

Elgendi, H., Sharshar, A., Aboeitta, A., Ashraf, Y., Guizani, M., 2024. Geollava: Efficient fine-tuned vision-language models for temporal change detection in remote sensing. *arXiv preprint arXiv:2410.19552*.

European Environment Agency, 2016. Biogeographical regions. European Environment Agency Datahub. Dataset published on 26 Jan 2016, last modified 30 Apr 2025.

European Environment Agency, 2019. Ecosystem types of europe 2012 – terrestrial habitats – version 3 revision 1, feb. 2019. European Environment Agency Spatial Data Catalogue. Dataset published on 31 Dec 2018, last modified on 27 Apr 2021.

He, K., Fan, H., Wu, Y., Xie, S., Girshick, R., 2020. Momentum contrast for unsupervised visual representation learning. *Proceedings of the IEEE/CVF conference on computer vision and pattern recognition*, 9729–9738.

Jain, P., Ienco, D., Interdonato, R., Berchoux, T., Marcos, D., 2025. Senclip: Enhancing zero-shot land-use mapping for sentinel-2 with ground-level prompting. *2025 IEEE/CVF Winter Conference on Applications of Computer Vision (WACV)*, IEEE, 5656–5665.

Keith, D. A., Ferrer-Paris, J. R., Nicholson, E., Bishop, M. J., Polidoro, B. A., Ramirez-Llodra, E., Tozer, M. G., Nel, J. L., Mac Nally, R., Gregr, E. J. et al., 2022. A function-based typology for Earth’s ecosystems. *Nature*, 610(7932), 513–518.

Klemmer, K., Rolf, E., Robinson, C., Mackey, L., Rußwurm, M., 2025. Satclip: Global, general-purpose location embeddings with satellite imagery. *Proceedings of the AAAI Conference on Artificial Intelligence*, 39number 4, 4347–4355.

Koldasbayeva, D., Tregubova, P., Gasanov, M., Zaytsev, A., Petrovskaya, A., Burnaev, E., 2024. Challenges in data-driven geospatial modeling for environmental research and practice. *Nature Communications*, 15(1), 10700.

Lausch, A., Bannehr, L., Beckmann, M., Boehm, C., Feilhauer, H., Hacker, J., Heurich, M., Jung, A., Klenke, R., Neumann, C. et al., 2016. Linking Earth Observation and taxonomic, structural and functional biodiversity: Local to ecosystem perspectives. *Ecological Indicators*, 70, 317–339.

Levering, A., Marcos, D., Jacobs, N., Tuia, D., 2024. Prompt-guided and multimodal landscape scenicness assessments with vision-language models. *PloS one*, 19(9), e0307083.

Levering, A., Marcos, D., Tuia, D., 2021. On the relation between landscape beauty and land cover: A case study in the UK at Sentinel-2 resolution with interpretable AI. *ISPRS journal of Photogrammetry and Remote Sensing*, 177, 194–203.

Li, Z., Xu, D., Guo, X., 2014. Remote sensing of ecosystem health: opportunities, challenges, and future perspectives. *Sensors*, 14(11), 21117–21139.

Liu, F., Chen, D., Guan, Z., Zhou, X., Zhu, J., Zhou, J., 2023. RemoteCLIP: A Vision Language Foundation Model for Remote Sensing. *arXiv preprint arXiv:2306.11029*.

Liu, Z., Zhang, F., Jiao, J., Lao, N., Mai, G., 2025. GAIR: Improving Multimodal Geo-Foundation Model with Geo-Aligned Implicit Representations. *arXiv preprint arXiv:2503.16683*.

Lu, X., Wang, B., Zheng, X., Li, X., 2017. Exploring models and data for remote sensing image caption generation. *IEEE Transactions on Geoscience and Remote Sensing*, 56(4), 2183–2195.

Mall, U., Phoo, C. P., Liu, M. K., Vondrick, C., Hariharan, B., Bala, K., 2023. Remote sensing vision-language foundation models without annotations via ground remote alignment. *arXiv preprint arXiv:2312.06960*.

Marimo, C. T., Blumenstiel, B., Nitsche, M., Jakubik, J., Brunschwiler, T., 2025. Beyond the visible: Multispectral vision-language learning for earth observation. *arXiv preprint arXiv:2503.15969*.

Pesaresi, S., Mancini, A., Quattrini, G., Casavecchia, S., 2022. Functional analysis for habitat mapping in a special area of conservation using sentinel-2 time-series data. *Remote Sensing*, 14(5), 1179.

Pettorelli, N., Wegmann, M., Skidmore, A., Mücher, S., Dawson, T. P., Fernandez, M., Lucas, R., Schaepman, M. E., Wang, T., O'Connor, B. et al., 2016. Framing the concept of satellite remote sensing essential biodiversity variables: challenges and future directions. *Remote sensing in ecology and conservation*, 2(3), 122–131.

Qiu, C., Zhang, X., Tong, X., Guan, N., Yi, X., Yang, K., Zhu, J., Yu, A., 2024. Few-shot remote sensing image scene classification: Recent advances, new baselines, and future trends. *ISPRS Journal of Photogrammetry and Remote Sensing*, 209, 368–382.

Qu, B., Li, X., Tao, D., Lu, X., 2016. Deep semantic understanding of high resolution remote sensing image. *2016 International conference on computer, information and telecommunication systems (Cits)*, IEEE, 1–5.

Radford, A., Kim, J. W., Hallacy, C., Ramesh, A., Goh, G., Agarwal, S., Sastry, G., Askell, A., Mishkin, P., Clark, J. et al., 2021. Learning transferable visual models from natural language supervision. *International conference on machine learning*, PMLR, 8748–8763.

Reichstein, M., Camps-Valls, G., Stevens, B., Jung, M., Denzler, J., Carvalhais, N., Prabhat, F., 2019. Deep learning and process understanding for data-driven Earth system science. *Nature*, 566(7743), 195–204.

Rußwurm, M., Körner, M., 2018. Multi-temporal land cover classification with sequential recurrent encoders. *ISPRS International Journal of Geo-Information*, 7(4), 129.

Sastry, S., Khanal, S., Dhakal, A., Ahmad, A., Jacobs, N., 2025. Taxabind: A unified embedding space for ecological applications. *2025 IEEE/CVF Winter Conference on Applications of Computer Vision (WACV)*, IEEE, 1765–1774.

Seresinhe, C. I., Preis, T., Moat, H. S., 2015. Quantifying the impact of scenic environments on health. *Scientific reports*, 5(1), 16899.

Shabbir, A., Zumri, M., Bennamoun, M., Khan, F. S., Khan, S., 2025. GeoPixel: Pixel Grounding Large Multimodal Model in Remote Sensing. *arXiv preprint arXiv:2501.13925*.

Sharma, S., Sedona, R., Riedel, M., Cavallaro, G., Paris, C., 2024. Sen4map: Advancing mapping with sentinel-2 by providing detailed semantic descriptions and customizable land-use and land-cover data. *IEEE Journal of Selected Topics in Applied Earth Observations and Remote Sensing*.

Soni, S., Dudhane, A., Debary, H., Fiaz, M., Munir, M. A., Danish, M. S., Fraccaro, P., Watson, C. D., Klein, L. J., Khan, F. S. et al., 2024. Earthdial: Turning multi-sensory earth observations to interactive dialogues. *arXiv preprint arXiv:2412.15190*.

Soubry, I., Doan, T., Chu, T., Guo, X., 2021. A systematic review on the integration of remote sensing and GIS to forest and grassland ecosystem health attributes, indicators, and measures. *Remote Sensing*, 13(16), 3262.

Tan, X., Xi, B., Li, J., Zheng, T., Li, Y., Xue, C., Chanussot, J., 2024. Review of zero-shot remote sensing image scene classification. *IEEE Journal of Selected Topics in Applied Earth Observations and Remote Sensing*.

Tschannen, M., Gritsenko, A., Wang, X., Naeem, M. F., Alabdulmohsin, I., Parthasarathy, N., Evans, T., Beyer, L., Xia, Y., Mustafa, B. et al., 2025. Siglip 2: Multilingual vision-language encoders with improved semantic understanding, localization, and dense features. *arXiv preprint arXiv:2502.14786*.

Vivanco Cepeda, V., Nayak, G. K., Shah, M., 2023. Geoclip: Clip-inspired alignment between locations and images for effective worldwide geo-localization. *Advances in Neural Information Processing Systems*, 36, 8690–8701.

Wang, Y., Xiong, Z., Liu, C., Stewart, A. J., Dujardin, T., Bountos, N. I., Zavras, A., Gerken, F., Papoutsis, I., Leal-Taixé, L. et al., 2025. Towards a Unified Copernicus Foundation Model for Earth Vision. *arXiv preprint arXiv:2503.11849*.

Wang, Z., Prabha, R., Huang, T., Wu, J., Rajagopal, R., 2024. Skyscript: A large and semantically diverse vision-language dataset for remote sensing. *Proceedings of the AAAI Conference on Artificial Intelligence*, 38number 6, 5805–5813.

Workman, S., Souvenir, R., Jacobs, N., 2017. Understanding and mapping natural beauty. *Proceedings of the IEEE International Conference on Computer Vision*, 5589–5598.

Zermatten, V., Castillo-Navarro, J., Jain, P., Tuia, D., Marcos, D., 2025. EcoWikiRS: Learning Ecological Representation of Satellite Images from Weak Supervision with Species Observations and Wikipedia. *arXiv preprint arXiv:2504.19742*.

Zhang, L., Zhang, L., Du, B., 2016. Deep learning for remote sensing data: A technical tutorial on the state of the art. *IEEE Geoscience and remote sensing magazine*, 4(2), 22–40.

Zhang, Z., Zhao, T., Guo, Y., Yin, J., 2023. Rs5m: A large scale vision-language dataset for remote sensing vision-language foundation model. *arXiv preprint arXiv:2306.11300*.

Zhong, L., Hu, L., Zhou, H., 2019. Deep learning based multi-temporal crop classification. *Remote Sensing of Environment*, 221, 430–443.

Zhu, X. X., Tuia, D., Mou, L., Xia, G.-S., Zhang, L., Xu, F., Fraundorfer, F., 2017. Deep learning in remote sensing: A comprehensive review and list of resources. *IEEE geoscience and remote sensing magazine*, 5(4), 8–36.